

ARMY RESEARCH LABORATORY



Design and Test of a Prototype Acoustic High-Intensity Infrasonic Test Chamber

H. Edwin Boesch, Jr., Bruce T. Benwell, and Christian G. Reiff

ARL-TR-2137

April 2000

Approved for public release; distribution unlimited.

DTIC QUALITY INSPECTED 1

20000525 041

The findings in this report are not to be construed as an official Department of the Army position unless so designated by other authorized documents.

Citation of manufacturer's or trade names does not constitute an official endorsement or approval of the use thereof.

Destroy this report when it is no longer needed. Do not return it to the originator.

Army Research Laboratory

Adelphi, MD 20783-1197

ARL-TR-2137

April 2000

Design and Test of a Prototype Acoustic High-Intensity Infrasonic Test Chamber

H. Edwin Boesch, Jr., Bruce T. Benwell, and Christian G. Reiff

Sensors and Electron Devices Directorate

Sponsored by
TACOM/ARDEC

Picatinny Arsenal
Dover, NJ 07806-3000

Approved for public release; distribution unlimited.

Abstract

We describe the conception, design, mathematical modeling, construction, and test of a prototype acoustic test chamber intended to support the performance of high-intensity acoustic target-effects experiments on large targets at infrasonic frequencies. In initial experiments, the test chamber produced continuous sinusoidal sound pressure levels in excess of 140 dB over a frequency range of 5 to 20 Hz within a test volume of 5 m³.

Contents

| | |
|--|----|
| 1. Introduction | 1 |
| 2. Proposed Acoustic Test Chamber | 2 |
| 3. Theoretical Response of Test Chamber | 5 |
| 4. Analysis of Chamber Wall Losses | 8 |
| 5. Construction of Prototype Test Chamber | 10 |
| 6. Instrumentation for Chamber Response Experiments | 13 |
| 7. Initial Chamber Response Experiment | 15 |
| 8. Chamber Wall-Stiffening Experiment | 21 |
| 9. Loudspeaker Drive Experiment | 24 |
| 10. Optimizing the Acoustic Intensity Within the Chamber | 26 |
| 11. Conclusions | 28 |
| Acknowledgments | 29 |
| References | 29 |
| Distribution | 31 |
| Report Documentation Page | 33 |

Figures

| | |
|--|----|
| 1. Sketch of proposed infrasonic test chamber | 3 |
| 2. Electrical circuit used to model the test chamber, source, and ports | 3 |
| 3. Predicted and measured response of prototype test chamber with 23-in.-diam, 4-in.-long port attached | 5 |
| 4. ANSYS finite-difference calculation for sound pressure at 17.86 Hz in prototype test chamber with 23-in.-diam, 4-in.-long port | 7 |
| 5. Experimentally derived and extrapolated absorption coefficients used to determine value of R_{wall} | 8 |
| 6. Concrete test chamber, ports, and MOAS modulator and air source used during experiments | 11 |
| 7. Detail of test chamber showing 1-ft ² , 30-in.-long port, modulator mounted at access hatch openings | 12 |
| 8. Waveform of acoustic signal in chamber with 23-in.-diam, 4-in.-long port attached and using 18 Hz excitation | 16 |
| 9. Spectrum of acoustic signal in chamber with 23-in.-diam, 4-in.-long port attached and using 18 Hz excitation | 16 |
| 10. Predicted and measured response of prototype test chamber with 1-ft ² , 54-in.-long port attached | 16 |
| 11. Spectrum of acoustic signal in chamber with 1-ft ² , 54-in.-long port attached and using 5.8 Hz excitation | 17 |

Figures (cont'd)

| | |
|--|----|
| 12. Comparison of predicted and measured natural resonant frequency of acoustic test chamber for various port configurations | 17 |
| 13. Comparison of predicted and measured sound pressure level inside test chamber for various port configurations | 18 |
| 14. Comparison of predicted and measured half-power bandwidth at resonance for various port configurations | 18 |
| 15. Comparison of measured sound pressure level inside test chamber with model predictions modified to reflect experimentally derived absorption coefficient | 19 |
| 16. Comparison of measured response of the chamber with 23-in.-diam, 4-in.-long port attached before and after the chamber was stiffened with steel rods | 22 |
| 17. A portion of FFTs of chamber wall accelerometer signals indicating magnitude of the chamber sound pressure level at 18 Hz and responses of the accelerometers to this force | 23 |
| 18. Measured and modeled response of chamber with closed port excited by JBL 18-in. loudspeaker. Jagged solid curve is measured response; smooth curves are model responses calculated with initial and modified chamber absorption..... | 25 |
| 19. Electrical circuit analog of chamber driven by loudspeaker used for model calculations..... | 25 |
| 20. Measured and modeled response of the chamber with 23 in. diam, 4-in.long port excited by JBL 18-in. loudspeaker | 25 |
| 21. Acoustic impedance of chamber when tuned to 18 Hz | 27 |
| 22. Volume flow and equivalent resistance of WAS 3000 air flow modulator as function of input pressure | 27 |

Tables

| | |
|---|----|
| 1. Predicted response of a $5 \times 5 \times 6.75$ ft concrete test chamber when excited by a modulated dc airflow at 6 psig and 1200 cfm | 6 |
| 2. Measured response for the $5 \times 5 \times 6.75$ ft prototype concrete test chamber when excited by a modulated dc air flow at 6 psig nominal and 1200 cfm | 17 |
| 3. Peak measured wall acceleration at 18 Hz values and resulting calculated power loss in chamber walls | 23 |
| 4. Summary of measured and projected test chamber results | 28 |

1. Introduction

For several years, the Department of Defense Joint Non-lethal Weapons Directorate, through the U.S. Army Close Combat Armaments Center at the Tank-Automotive and Armaments Command/Armament Research, Development and Engineering Center (TACOM/ARDEC), has sponsored an effort—the Nonlethal Acoustic Weapons (NLAWs) program—to demonstrate acoustic technologies that may be useful for nonlethal weapons. The U.S. Army Research Laboratory (ARL) Nonlethal Acoustics Group has supported the NLAWs program with field and laboratory measurements, technical advice, and research into the design of high-intensity acoustic sources. Of particular interest for NLAW applications are the effects of sound at very low audible or subaudible (infrasonic) frequencies.

The generation of controllable and intense infrasound is a difficult problem. The very large wavelengths involved render most sources of high-intensity sound (such as loudspeakers, sirens, or horn-coupled flow modulators) inefficient or completely ineffective at frequencies below a few tens of hertz.

2. Proposed Acoustic Test Chamber

In May 1998, the ARL acoustics team in consultation with ARDEC staff addressed the problem of designing an acoustic test facility for acoustic effects experiments. This conceptual facility would consist of a test chamber and an associated source of acoustic energy. The goals for the test facility design included (1) a test volume sufficient to hold test items and associated experimental apparatus (about 5 m³), (2) a frequency range capability from the lower audible range (about 20 Hz) down to the single-digit infrasonic range (about 5 Hz), and (3) a uniform sound field in the chamber with an accurately controllable intensity up to 160 dB.

The starting point for our design was some form of closed chamber driven by acoustic energy from a flow modulator (to be provided by ARDEC) and a compressed air source. A flow modulator is, in essence, a valve that creates acoustic energy from a continuous airflow by varying that flow with an aperture controlled by an electrical signal. As opposed to loudspeaker sources that are limited to acoustic intensities near 140 dB, flow modulators are capable of intensities limited only by the available air pressure and atmospheric nonlinearities. As a matter of necessity (to limit the exposure of personnel to high-intensity sound) and convenience (a controlled, accessible, and weather-independent environment), acoustic-effects experiments generally employ closed exposure chambers. In addition, closed chambers make possible the concentration of the acoustic energy in a small volume and offer the potential of increased acoustic intensities from sources of limited power. Use of a closed chamber also makes possible the amplification of acoustic intensities by tuning the chamber to resonate at the desired frequency.

There are two types of resonant acoustic chambers: resonance tubes and Helmholtz resonators. The former operate at wavelengths no greater than half their major dimension: to operate at 10 Hz, a chamber would have to be at least 16 m long. In addition, resonance tubes by nature produce a highly nonuniform sound field (standing wave). On the other hand, Helmholtz resonators operate at wavelengths greater than their largest dimensions and produce uniform sound fields throughout the resonant volume. After numerous brainstorming sessions, we decided that the ideal *infrasonic* test chamber would take advantage of the high gain present within a Helmholtz resonator yet have the frequency tunability of a ported bass reflex enclosure. The test chamber would consist of a structurally massive test chamber of moderate volume with a port vented to free space and tunable for frequency selectability. The acoustic power source to drive this chamber would be a high-flow dc air supply modulated by an airflow modulator. We anticipated that sound pressures of 160 dB over a frequency range from 3 to 20 Hz would be achievable. Figure 1 is a sketch of the proposed chamber.

To evaluate the feasibility of this ported test chamber-Helmholtz resonator, we modeled the overall system taking advantage of the fact that, since we were working at infrasonic frequencies, the dimensions of the chamber and ports are necessarily small compared to the acoustic wavelength. This wavelength-to-chamber dimensional relationship allowed for a significant simplification in modeling the response of the chamber since acoustic lumped elements could be used to represent the reactive (energy storage) and loss (dissipation) elements. Standard circuit analysis techniques could then be employed to theoretically predict the frequency response and sound pressure level (SPL) within the chamber.

Figure 2 shows the electrical circuit used to model the response of the source, chamber, and ports. In this model, loss elements (port radiation, viscous losses within the port, and wall-absorption losses) are modeled as resistors. Air-mass displacement terms are modeled as inductors, and the compressed air volume within the chamber is modeled as an acoustic compliance or capacitance. The magnitude of the acoustic intensity inside the chamber is simply the voltage across the chamber compliance/capacitor C_{ac} . The magnitudes of the following circuit elements were derived either by hand or from Beranek [1] or Seto [2].

Figure 1. Sketch of proposed infrasonic test chamber.

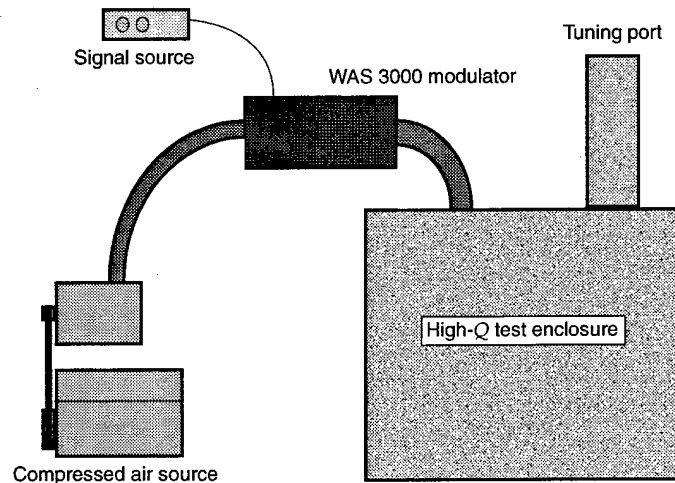
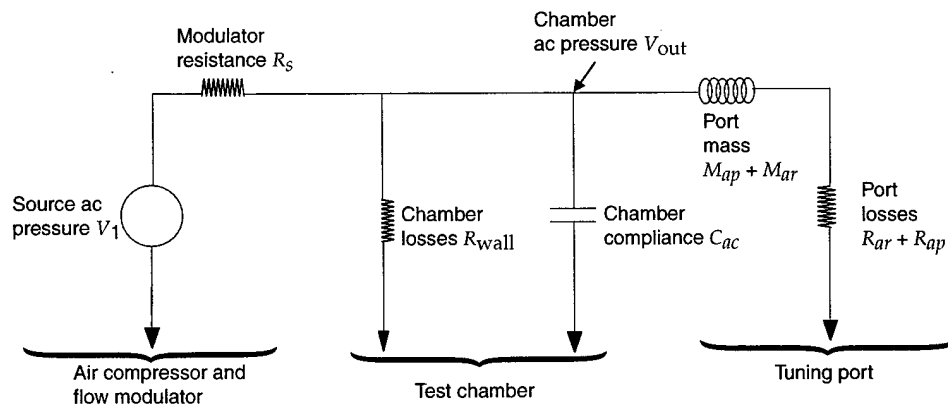


Figure 2. Electrical circuit used to model the test chamber, source, and ports.



The source terms are as follows: The equivalent source resistance R_s in pascals per meters cubed per second is

$$R_s = P_1/v, \quad (1)$$

where

P_1 = source pressure in pascals, and
 v = volume velocity in meters cubed per second.

The chamber terms are as follows: The chamber compliance C_{ac} in meters to the fifth power per newton is

$$C_{ac} = V/(\rho c^2), \quad (2)$$

where

V = chamber volume,
 ρ = density, and
 c = speed of sound.

The losses through the walls R_{wall} is

$$R_{wall} = (2\gamma P_o)/(cC_{abs}S), \quad (3)$$

where

γ = specific heat = 1.4,
 P_o = atmospheric pressure in pascals,
 C_{abs} = wall-absorption coefficient, and
 S = wall surface area.

The port terms seen by the chamber are as follows: The mass of air in the port M_{ap} in kilograms per meter to the fourth power is

$$M_{ap} = (L + 0.6 a_2) \rho / (\pi a_2^2), \quad (4)$$

where

a_2 = radius of port, and
 L = port length.

R_{ap} is the viscous losses in the port:

$$R_{ap} ((L/a_2) + 1) = (1/(\pi a_2^2)) \rho (2 \omega \mu)^{1/2}, \quad (5)$$

where

$\omega = 2\pi f$,
 μ = kinetic coefficient of friction = 1.56×10^{-5} m²/s at 20 °C and 0.76 mm Hg, and
 f = frequency.

The port terms exterior to the chamber are as follows: The acoustic mass of the front side of port M_{ar} in kilograms per meter to the fourth power is

$$M_{ar} = 0.23/a_2, \quad (6)$$

and the radiation resistance R_{ar} is

$$R_{ar} = (\pi f^2 \rho)/c. \quad (7)$$

3. Theoretical Response of Test Chamber

The circuit shown in figure 2 can be thought of as a simple parallel resistor-inductor-capacitor (RLC) circuit. If one solves the circuit equations with the actual component values, this will show that the circuit response is underdamped and, further, that the circuit forced response simplifies to a single exponential function with a damping factor a equal to $\frac{R_{eff} C_{ac}}{2}$, where R_{eff} is the effective loss term from all the chamber and port losses. The natural resonant frequency of the chamber and port combination (in radians) is

$$\omega_d = (\omega_o^2 - a^2)^{1/2}, \quad (8)$$

where $\omega_o = 1/(M_{eff} C_{ac})^{1/2}$ and M_{eff} is the effective total acoustic mass of the port (both internal and external terms).

A typical theoretical response for the circuit is shown by the upper smooth solid curve in figure 3. For this case, the chamber consists of a $5 \times 5 \times 6.75$ ft tank with a 23-in.-diam, 4-in. long port, which is driven by a modulated dc air supply of 6 psig (peak) at 1200 cfm. The response is characterized by a resonant peak occurring at the natural resonant frequency. The equation for ω_d shows that the natural resonant frequency is dominated by the reactive components in the circuit. Since the chamber volume C_{ac} is fixed, varying the length and, therefore, the inductance of the port adjusts the resonant frequency. Table 1 summarizes the amplitude and resonant frequencies to be expected from a $5 \times 5 \times 6.75$ ft concrete chamber for some typical port dimensions. Also shown in the table is the half-power bandwidth and corresponding Q for the chamber, which is determined from the width of the resonance in the calculated circuit

Figure 3. Predicted and measured response of prototype test chamber with 23-in.-diam, 4-in.-long port attached. Upper solid smooth curve is predicted response based on electrical analog model in figure 2. Jagged solid curve is actual measured response of chamber. Other curves are model response calculations altered to fit measured response.

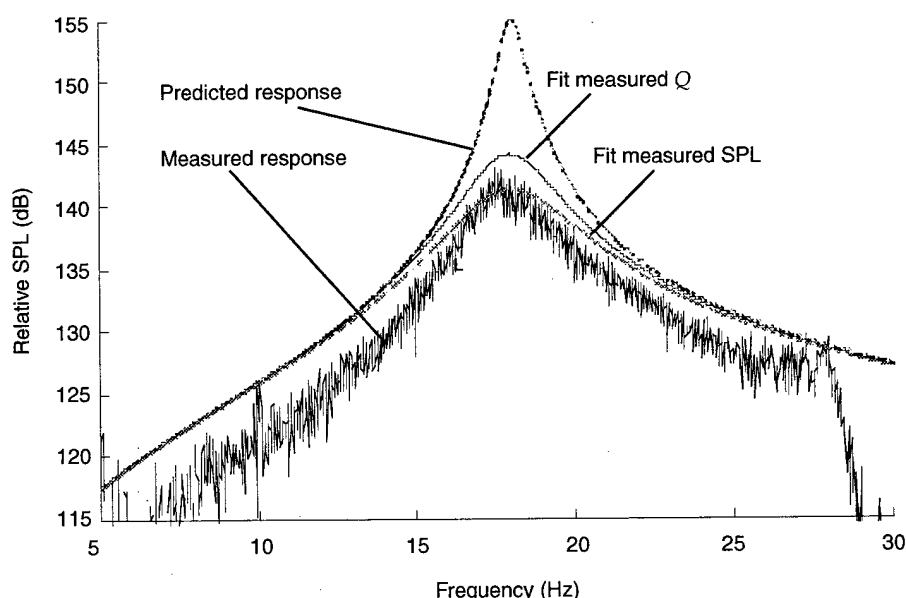


Table 1. Predicted response of a 5 × 5 × 6.75 ft concrete test chamber when excited by a modulated dc airflow at 6 psig (peak) and 1200 cfm.

| Port shape | Size of opening | Length (in.) | Resonant frequency (Hz) | Maximum amplitude (dB) | Half-power bandwidth (Hz)/Q |
|------------|-------------------|--------------|-------------------------|------------------------|-----------------------------|
| Circular | 23-in. diam | 4 | 18.1 | 153.1 | 0.9/20.1 |
| Square | 1 ft ² | 30 | 7.6 | 155.7 | 0.5/15.2 |
| Square | 1 ft ² | 54 | 5.9 | 157.2 | 0.5/11.8 |

Note: The dc pressure values have been corrected by ac pressure fluctuations measured at the modulator inlet.

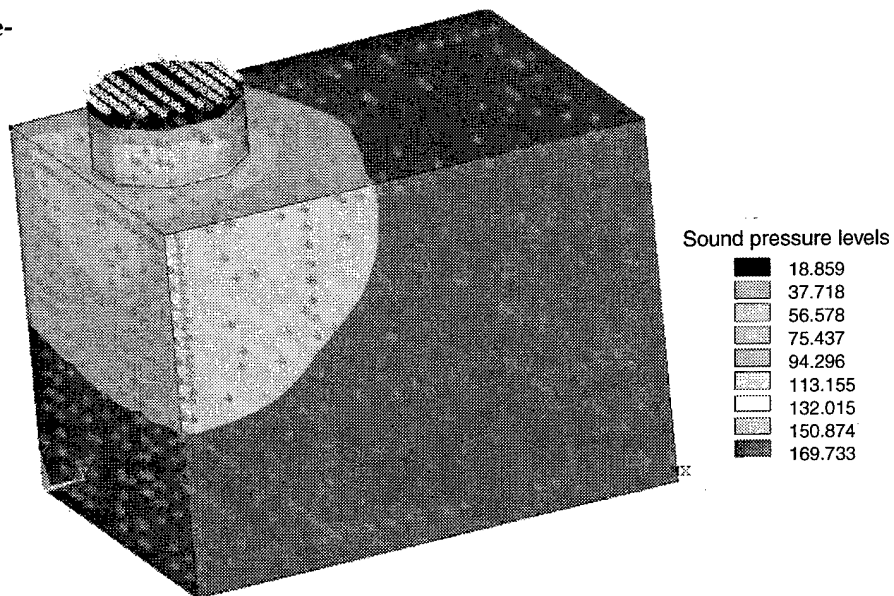
response. Q is a measure of the ability of the chamber to *store* acoustic energy; it is the ratio of the energy density in the chamber to the energy lost per cycle at the resonant frequency. Q is affected directly by the chamber and port loss terms, since these terms represent the mechanisms by which acoustic power is lost from the system.

Here, we summarize some of the trends predicted by the model:

1. The resonant frequency is inversely related to the square of the chamber volume (smaller volumes generate higher resonant frequencies).
2. The resonant frequency is proportional to the square of the port area (larger port areas generate higher resonant frequencies).
3. The resonant frequency is inversely proportional to the square of the port length (larger port lengths generate lower resonant frequencies). In other words, if you want to increase the resonant frequency of a given size chamber, you want to add ports with large diameters and short lengths.
4. The acoustic intensity in the chamber is maximized by minimizing the equivalent modulator impedance (the source should produce a high flow at low pressure with minimal restriction in the modulator).

Our first attempt at validating our lumped circuit model was to compare our predictions to the theoretical response predicted using an ANSYS physics software model [3]. The ANSYS model provided an excellent unbiased comparison since ANSYS is a finite element modeling package for solving the acoustic wave equations and did not use the lumped circuit models for the chamber elements derived for our calculations. Figure 4 shows the ANSYS prediction for the sound pressure in the 5 × 5 × 6.75 ft chamber and 23-in.-diam port combination discussed above (see fig. 3 and table 1) when this chamber is driven by an acoustic signal at 17.86 Hz. The resonant frequency predicted by the ANSYS model is in excellent agreement with our lumped circuit model and provides independent validation of the reactive elements in that model. As expected, the figure also shows that the predicted SPL inside the chamber is nearly uniform at resonance. Unfortunately, the ANSYS model cannot accurately treat either the acoustic energy source and its coupling to the chamber or the loss elements in the model and, therefore, cannot accurately estimate the absolute intensity.

Figure 4. ANSYS finite-difference calculation for sound pressure at 17.86 Hz in prototype test chamber with 23-in.-diam, 4-in.-long port.



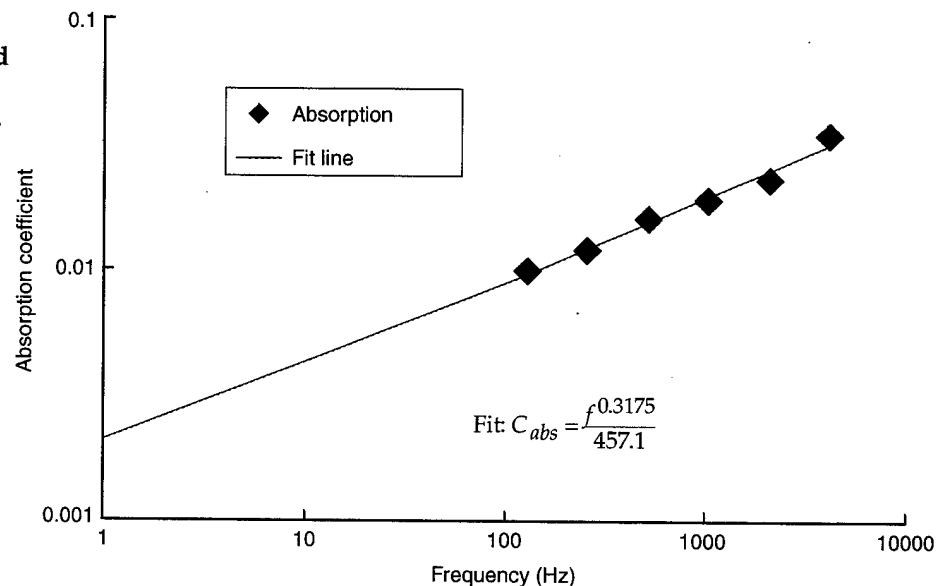
4. Analysis of Chamber Wall Losses

Equation (3), which defines R_{wall} , is based on the acoustic absorption (or absorption coefficient) C_{abs} of the inner wall surfaces. The absorption coefficient is simply a decimal fraction representation of perfect sound absorption (i.e., $C_{\text{abs}} = 0.1$ means 10 percent absorption). The absorption coefficient generally decreases with decreasing frequency.

The absorption coefficient used for our model was based on data for unpainted concrete walls measured over a frequency range from 128 to 4096 Hz [4]. A frequency-dependent equation was then derived to extrapolate these data to the frequencies of interest to our investigation (<20 Hz). Figure 5 shows the experimentally derived absorption coefficients from Olson [4] as well as the extrapolated curve used to determine the value of R_{wall} at lower frequencies. This figure shows that the extrapolated absorption coefficients are 0.35, 0.39, and 0.56 percent at 5.8, 7.4, and 18.0 Hz, respectively. These extrapolated coefficients were then used to calculate the value of R_{wall} in the theoretical model used to predict the SPL within the chamber.

It is important to stress that at very low frequencies wall absorption is not necessarily the dominant loss term for a structure. At large wavelengths, the wall's structural integrity, rigidity, or stiffness cannot be ignored, and the work that goes into wall displacement (flexure) or vibration will dominate. The loss factor associated with wall integrity cannot be easily defined since it is uniquely dependent on the individual wall and fabrication process. Additional reference material located after the test chamber

Figure 5.
Experimentally derived
and extrapolated
absorption coefficients
used to determine
value of R_{wall} .



Source: H. F. Olson, *Acoustical Engineering*, Van Nostrand, Princeton, NJ (1957), p 502.

experiments were completed suggests that well-made (structurally rigid) enclosures exhibit a wall absorption that decreases with frequency (see fig. 5), with one exception. At low frequencies (a frequency value that cannot be easily predicted since it is unique to the structure in question), the coefficient flattens out to a constant value typically no less than approximately 1 percent. The frequency at which the coefficient tends to become constant is typically between 10 and 30 Hz.

5. Construction of Prototype Test Chamber

To validate the circuit model that we derived for the proposed test chamber, we constructed and then tested an experimental prototype. The ideal test chamber for these tests would be both infinitely massive and stiff to eliminate wall absorption and vibration losses at these extremely low frequencies. Since the ideal chamber is not achievable, we decided to use a precast concrete chamber in hopes that we could minimize wall absorption while providing enough structural integrity to minimize vibration losses. The chamber size ($5 \times 5 \times 6.75$ ft) was chosen as a compromise between the need to minimize the chamber size to maximize the resonant frequency yet maintain a large enough test volume to accommodate larger test subjects.

The chamber is actually a commercially available 1000-gal. grease trap, where the floor and four walls are tied together with No. 3 steel reinforcing rods (rebar) spaced 12 in. on center and then precast at one time with concrete. The concrete thickness is approximately 4 in. on the bottom and 3 in. on the walls. The chamber top or lid is cast as a separate piece and is approximately 4 in. thick. In addition to using the same concrete mix and rebar reinforcement found in the floor and walls, the lid is additionally reinforced with 6×6 in. No. 10 gauge wire mesh. The lid was sealed to the walls by a tar material placed around the top of the walls and compressed by the weight of the lid. The lid contains two 23-in.-diam manhole ports. The manholes were tapered from $22\frac{1}{2}$ in. at the bottom to 24 in. at the top with a ledge to receive a manhole cover. For the experimental tests, one access port was used to plumb in the air source while the second access port was used to attach the tuning ports. Instrumentation cables entered the chamber through a 2-in.-diam hole made in a 4-in.-diam knockout plug near the top edge of the end wall.

Two interchangeable 1-ft² tuning ports were constructed from $\frac{3}{4}$ in. exterior grade plywood. The ports were reinforced in the corners with 2×3 in. battens and fastened together with wood screws and construction adhesive. These tuning ports were then mounted to one of the chamber manholes with an adapter made of a 4×3 ft sheet of $\frac{3}{4}$ in. plywood with a 1-ft² opening and an attached 6-in.-long tuning port. A skirt on one end of the longer tuning ports would slip over the 6-in.-long port on the adapter, resulting in tuning ports with total lengths of 30 and 54 in. The adapter was attached to the access manhole by long bolts that passed through the manhole to two 2×4 in. boards positioned across the underside of the manhole. An airtight seal was formed between the top of the chamber and the adapter by a sheet of $\frac{3}{4}$ in. foam board compressed between the adapter and the chamber with the bolts.

The flow modulator was mounted on the inlet manhole with a similar adapter. This adapter consisted of a cradle cut from 2×4 in. material to fit the modulator and mounted on a 4×3 ft plywood sheet. A hole was cut

in the plywood to accept the end of a 4-in.-ID pipe elbow connected to the output port of the modulator. The elbow was bolted at the 4-in.-diam hole in the adapter plywood sheet, the modulator was strapped to the cradle, and the whole assembly on the adapter plywood sheet was bolted through the manhole as described for the tuning port adapter.

The air source used to excite the chamber consisted of the dc air supply and air flow modulator from ARL's Mobile Acoustic Source (MOAS). The dc air supply is generated with a compressor driven by a diesel engine that maintains a preset constant air pressure at the input to the flow modulator. The airflow modulator is a Wyle Laboratories model WAS 3000. In essence, this modulator is a valve with an aperture that can be varied linearly about the 50-percent open position by the application of electrical waveforms with frequencies up to 300 Hz. The MOAS air source and Wyle modulator could be operated at pressures from 2.7 to 15.0 psig and corresponding dc air flow rates from 820 to 1890 cfm.

Figure 6 shows the concrete test chamber, ports, and MOAS source used during the experiments. The flow modulator can be seen attached to the lid of the chamber towards the back. A 30-in. port is attached to the chamber lid near the front. Immediately in front of the chamber on the ground is a 1-ft² × 54-in.-long port. The dc air compressor sits on the flatbed trailer behind the chamber but is outside the frame of the picture. Figure 7 shows a top view of the chamber lid with the WAS 3000 modulator at the right mounted on its cradle and adapter (note the air hose from the MOAS compressed air source) and the tuning port installed on the adapter at the left.

Figure 6. Concrete test chamber, ports, and MOAS modulator and air source used during experiments.

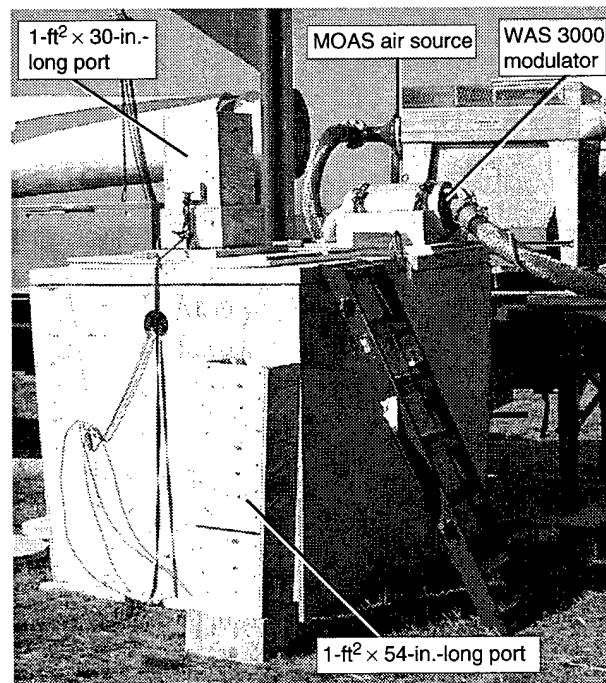
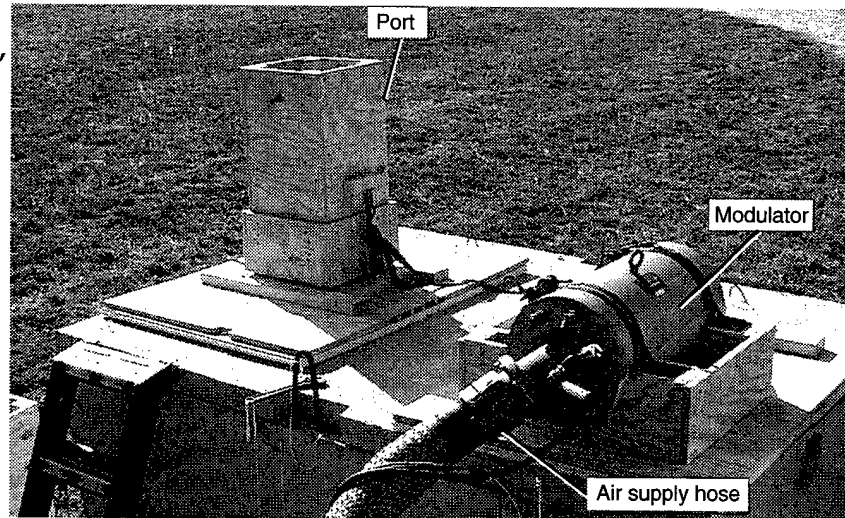


Figure 7. Detail of test chamber showing 1-ft², 30-in.-long port and modulator (with air source supply hose) mounted at access hatch openings.



6. Instrumentation for Chamber Response Experiments

To characterize the chamber, four simultaneous measurements were recorded in parallel on a digital audio tape (DAT) recorder, a digital oscilloscope, and a waveform digitizer attached to a laptop computer.

Channel 1 of the recorder monitored the instantaneous air pressure supplied to the modulator using a pressure transducer. This transducer was mounted in an adapter connected by a short vinyl tube transition to a fitting on the modulator inlet and secured with hose clamps.

Channel 2 monitored the pressure in the chamber using a microphone and preamplifier that were centered in the chamber 30 in. from the floor and walls and 32 in. from the end wall. (In the initial chamber response measurements, two microphones were in the chamber 30 in. from the floor and 24 in. from each end wall.) The microphone and preamplifier were mounted on a tripod and positioned perpendicular to the flow of air between the ports. The microphone cable was passed out of the chamber through a 2-in.-diam hole cut in an access knockout near the top end wall. An extension to the microphone cable brought the signal to the microphone and preamplifier power supply in the van. The signal was then routed to the data acquisition equipment in the van.

Channels 3 and 4 monitored accelerometers attached to the ceiling and long side wall of the chamber, respectively. The sensors were mounted inside the chamber near the center and perpendicular to the surface being monitored. The sensors were offset from the center of the wall panels by about 8 in. to allow room for the steel plates and braces used to stiffen the walls and ceiling (see sect. 9). The accelerometers were screwed to Plexiglas mounts glued to the surfaces with well-cured epoxy. The accelerometer cables were taped to the surfaces at intervals to prevent vibration noise, exited the chamber through the hole in the knockout, and were connected to the charge amplifiers positioned on a table located outside the chamber below the knockout. The signals from the charge amplifiers were sent to the van through 50-ft-long coaxial cables.

The instruments used for the measurements are listed below:

- DAT recorder, Sony, model PC204A.
- Digital oscilloscope, Tektronics model TDS684A.
- Waveform digitizer, IOtech Wavebook/512.
- Roof accelerometer, Bruel & Kjaer model 4375, calibration factor (CF) = 0.318 pC/ms^2 .
- Wall accelerometer, Bruel & Kjaer model 4375, $\text{CF} = 0.321 \text{ pC}/(\text{m/s}^2)$.
- Two charge amplifiers, Bruel & Kjaer model 2635, $0.1 \text{ mV}/(\text{m/s}^2)$.

- Pressure transducer, PCB model 113A24, 190.5 psig/V.
- ICP amp/supply, PCB model 482B11.
- Condenser microphone, Bruel & Kjaer model 4135, 278.55 Pa/V.
- Microphone preamplifier, Bruel & Kjaer model 2699.
- Dual microphone power supply, Bruel & Kjaer model 5935.
- Acoustic calibrator, Bruel & Kjaer model 4321.

7. Initial Chamber Response Experiment

We performed three experiments using the concrete chamber. The first experiment explored the acoustic response of the unmodified chamber driven by the MOAS air source and modulator with each of the various tuning ports and was intended to demonstrate *proof of principle* and verify the design model, including the theoretical lumped circuit model and the derivations for the individual circuit elements.

Figure 3 (p 5) shows the measured frequency response of the sound pressure inside the chamber when the chamber was driven by a sine wave swept from 5 to 50 Hz from the modulator with 6-psig input pressure and with the 23-in.-diam, 4-in.-long port in use (ragged solid curve). The observed resonant peak is at 18.3 Hz. This is within 2 percent of the calculated frequency of 18.0 Hz (solid smooth curve in figure). Near resonance, the chamber is uniformly filled (within 1 dB as measured approximately 2 ft above the floor) with a very pure acoustic sine wave; the waveform at 18.0 Hz is shown in figure 8. The spectral content of this waveform as obtained by fast Fourier transform (FFT) analysis is shown in figure 9. The second and third harmonics are more than 35 dB below the intensity of the fundamental at 18 Hz. At 18.3 Hz, 99.8 percent of the total acoustic energy is at the resonant frequency. Unfortunately, comparison of the measured and predicted response in figure 3 shows that the intensity of the measured sound pressure at resonance is approximately 15 dB less than anticipated. Also, in comparison to the initially predicted response, the measured response also shows a much wider peak at resonance, corresponding to a substantially larger bandwidth and a lower Q for the system than we predicted.

Figures 10 and 11 show results for equivalent tests using the 1-ft² × 54-in.-long port and 6-psig input pressure to the modulator. Here, the observed resonance is at 5.8 Hz (ragged solid curve in fig. 10); again, this is within the measurement error of the calculated resonant frequency. The FFT of the acoustic signal recorded at 5.8 Hz (fig. 11) confirms the purity of the waveform at resonance in the chamber. Again, we can observe in figure 10 that the measured intensity in the chamber at resonance is over 15 dB below the initially predicted level and that the measured bandwidth is greater than expected (Q is less than expected). Table 2 summarizes the results of these tests. The data from tables 1 and 2 are compared in figures 12 to 14. Figure 12 compares the predicted and measured resonant frequencies. This figure shows that the measured resonant frequencies are in almost exact agreement (within 2 percent) with the predicted value. This validates the derivation of each of the reactive elements in the model. However, as we have noted, figure 13 shows that the SPL measured for each port configuration is about 15 dB less than expected. Figure 14 shows that in each case the half-power bandwidth at resonance is substantially greater than expected.

Figure 8. Waveform of acoustic signal in chamber with 23-in.-diam, 4-in.-long port attached; 18-Hz excitation.

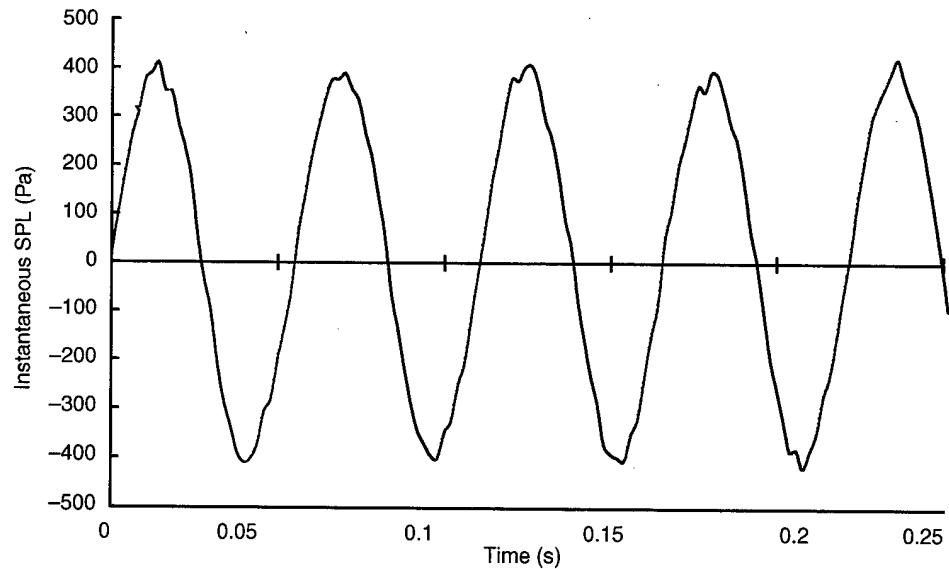


Figure 9. Spectrum of acoustic signal in chamber with 23-in.-diam, 4-in.-long port attached; 18-Hz excitation.

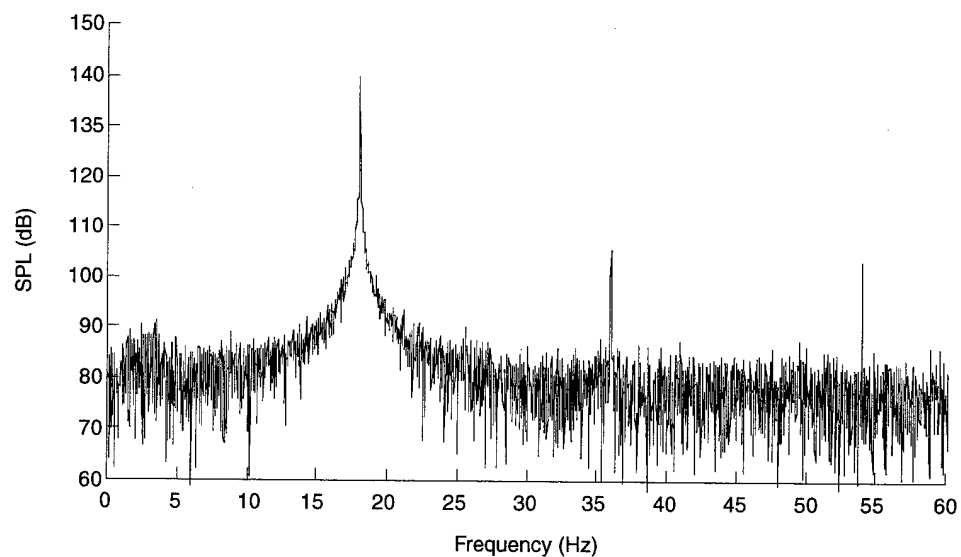


Figure 10. Predicted and measured response of prototype test chamber with 1-ft², 54-in.-long port attached. Upper solid smooth curve is predicted response based on electrical analog model in figure 2. Jagged solid curve is actual measured response of chamber. Other curves are model response calculations altered to fit measured response.

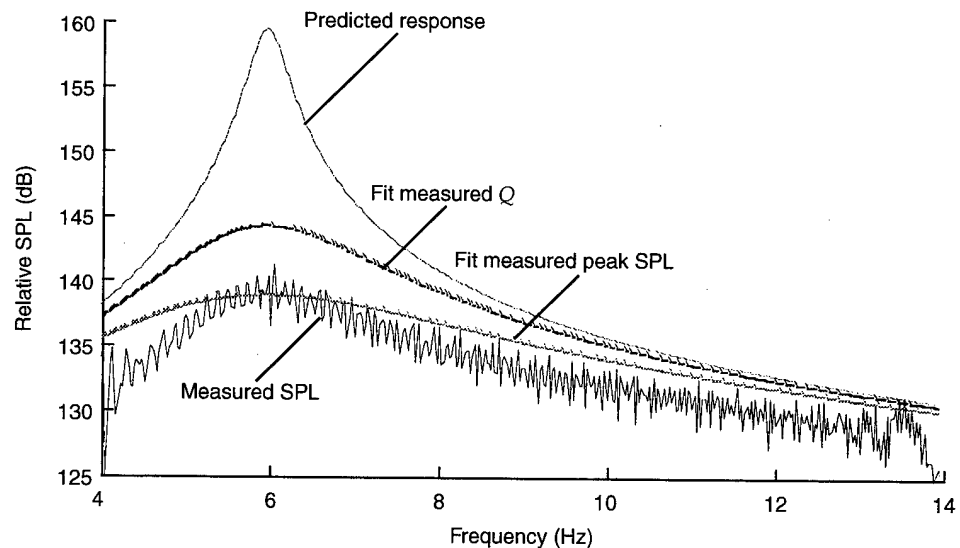


Figure 11. Spectrum of acoustic signal in chamber with 1-ft², 54-in.-long port attached; 5.8-Hz excitation.

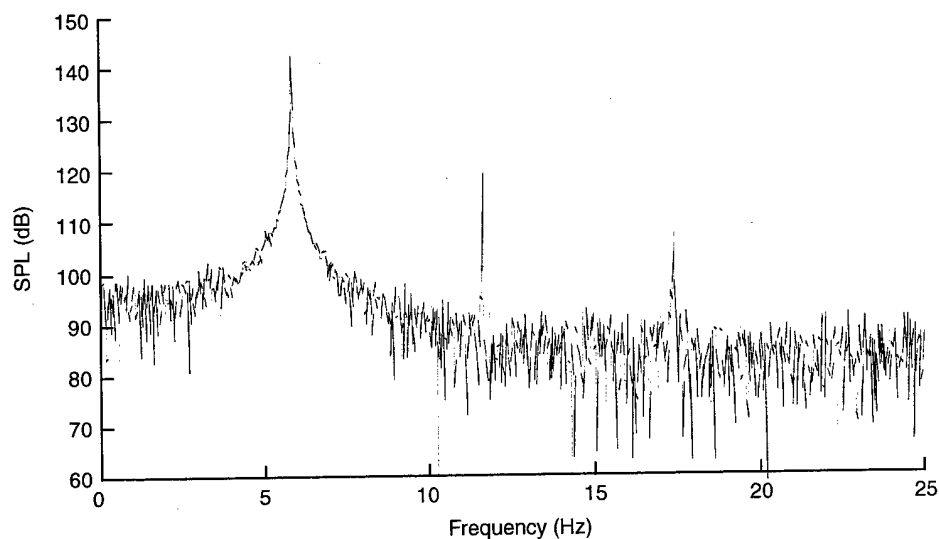


Table 2. Measured response for 5 × 5 × 6.75 ft prototype concrete test chamber when excited by a modulated dc air flow at 6 psig nominal and 1200 cfm.

| Port shape | Size of opening | Length (in.) | Resonant frequency (Hz) | Maximum amplitude (dB) | Half-power bandwidth (Hz)/Q |
|------------|-------------------|--------------|-------------------------|------------------------|-----------------------------|
| Circular | 23-in. diam | 4 | 18 | 143 | 2.7/ 6.7 |
| Square | 1 ft ² | 30 | 7.4 | 141.4 | 1.8/ 4.1 |
| Square | 1 ft ² | 54 | 5.9 | 141.7 | 2.0/ 2.95 |

Figure 12. Comparison of predicted and measured natural resonant frequency of acoustic test chamber for various port configurations.

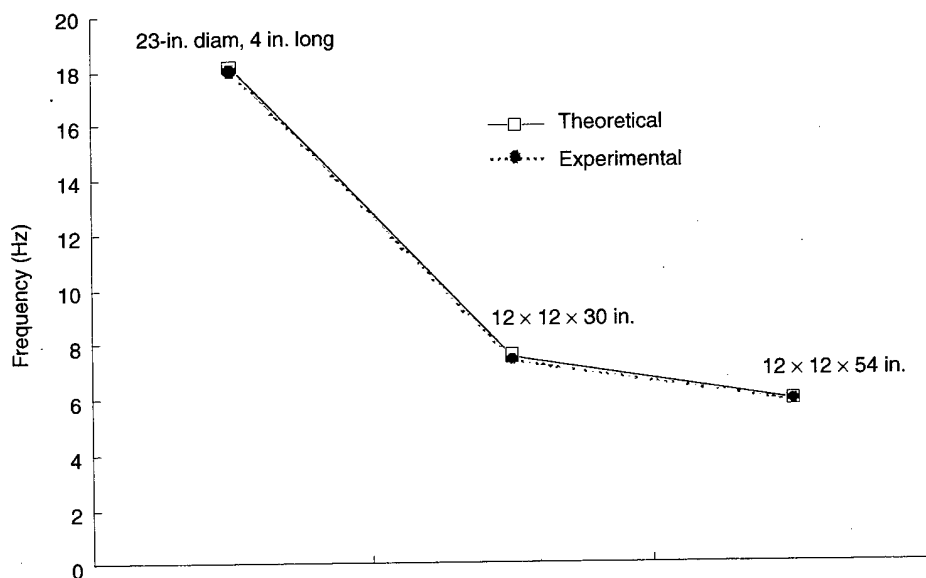


Figure 13. Comparison of predicted and measured sound pressure level inside test chamber for various port configurations.

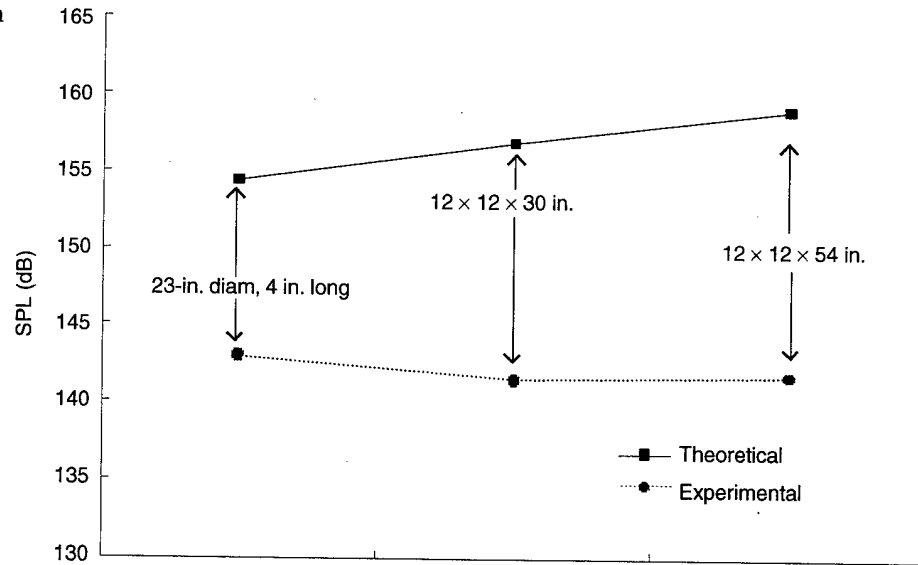
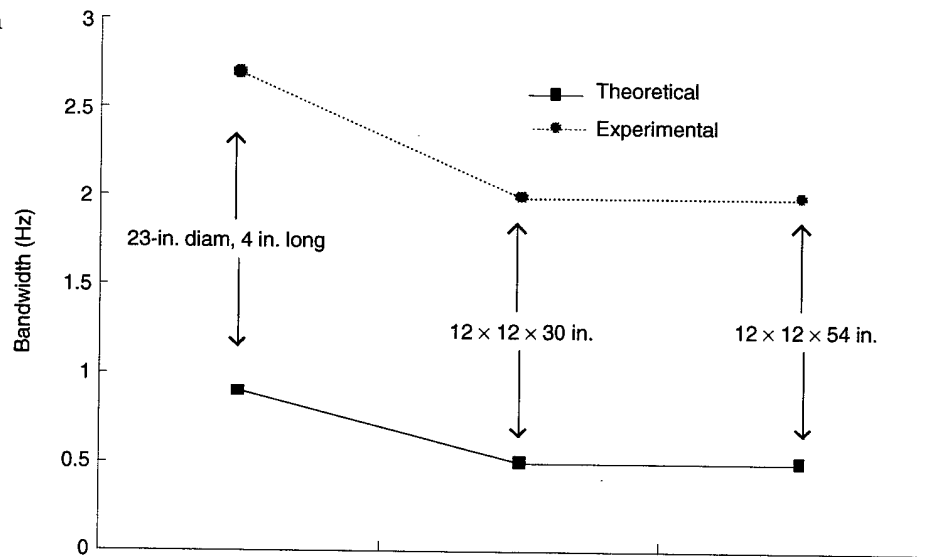


Figure 14. Comparison of predicted and measured half-power bandwidth at resonance for various port configurations.

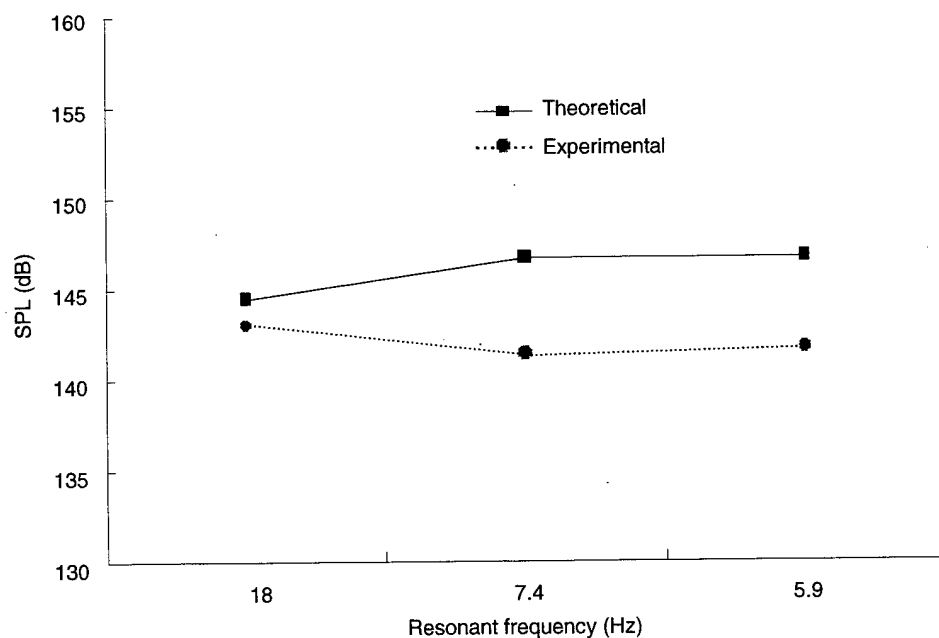


The discrepancies between the predicted and observed peak acoustic intensities and predicted and observed system bandwidths indicate that the system contains losses that we did not include in the initial model. In our model, increased chamber losses correspond to a reduced value for the parallel loss resistance (fig. 2). The dotted smooth curves in figures 3 and 10 correspond to system responses calculated with chamber losses adjusted to match the bandwidth (or Q) of the measured response. This adjustment also brings the modeled intensity at resonance into closer agreement with the observations. Thus, based on the experiments performed on the concrete test chamber, we can infer from the measured data that the actual equivalent absorption coefficients for the concrete chamber were 2.1, 1.9, and 2.2 percent at 5.8, 7.4, and 18.0 Hz,

respectively. These measured values are substantially (4 to 6 times) larger than our extrapolated values. When the experimentally derived absorption factors are incorporated back into our chamber circuit model (in effect we modified the theoretical half-power bandwidth or system Q to match the measured data), the comparison between the measured and predicted SPL is improved by nearly 10 dB (see fig. 15). The model still overestimates the intensity by up to 5 dB (at 5.8 Hz). To match the observed intensities at resonance, the loss term C_{abs} in the model was increased (which leads to R_{loss} being reduced) still more (the lowest dashed smooth curves in fig. 3 and 10). However, these curves are now too broad; i.e., they no longer fit the observed system bandwidth or Q . Evidently, the present model does not include some additional losses in the system that are not associated with the chamber; such losses would not affect the system Q . These losses may be associated with the modulator or with coupling of the acoustic signal into the chamber.

Nevertheless, our modeling suggests that the majority of the additional losses are accounted for by the observed change in system Q and are, therefore, attributable to the chamber. This additional chamber loss can occur as either a radiation loss from the port (R_{ar}), viscous loss through the port (R_{ap}), or losses associated with the chamber walls (R_{wall}). Because of the overall geometry of the port and chamber and the associated wavelength, it is very unlikely that there would be significant additional losses associated with either viscous and radiation losses other than what the model predicts. These loss values would need to be increased by orders of magnitude to account for the measured response of the chamber

Figure 15.
Comparison of
measured sound
pressure level inside
test chamber with
model predictions
modified to reflect
experimentally
derived absorption
coefficient.



(which is geometrically unfeasible). Following the first experiment, we hypothesized that the most likely source for the additional loss was absorption or transmission of energy by the chamber walls (see sect. 8).

An additional chamber loss term not accounted for in the model may result from the dc airflow from the modulator literally *blowing energy out the port*. At resonance, the chamber and port exchange acoustic energy in the form of the potential energy of air compression in the chamber and kinetic energy in the motion of the air mass in the port. If sound-induced kinetic energy in the port air mass is blown out of the port by the dc airflow such that it cannot react back on the chamber, that energy is lost to the system. Additional experiments described in section 9 detail a set of measurements to investigate this possible effect.

8. Chamber Wall-Stiffening Experiment

The actual absorption coefficient that we inferred from the initial chamber response experiment suggests that the coefficient for this chamber tended toward a constant value of approximately 2 to 3 percent, as opposed to a frequency-dependent loss of less than 1 percent as extrapolated from the literature (see fig. 5). This fact lends support to our hypothesis that the additional loss we measured is due to the structural integrity of the chamber. With this in mind, in a second set of experiments we attempted to increase the rigidity of the chamber by adding reinforcing and stiffening members. We also instrumented the chamber with accelerometers to measure deflections in the walls induced by the sound pressure.

The chamber was stiffened by the addition of heavy steel rods that tied together opposite walls to reduce symmetrical expansion and contraction (breathing mode) flexure of the chamber. To install the rods between the larger walls, we first drilled small holes through the centers of the top and bottom and larger (6 ft 9 in. \times 5 ft) sides. We then installed 1-in. cold-rolled steel rods between the top and bottom and larger sides with 1-ft² steel plates as washers on either side of the concrete walls. An epoxy-based paint was also applied to the interior of the chamber to increase the hardness of the inner wall surface.

Accelerometers were installed on the walls and lid to determine the degree of wall flexure. These accelerometers measured the movement of the side wall and lid during the experiment. The direction of the movement measured was perpendicular to the plane of the wall or lid. The purpose of the measurements was to determine the deflection or flex in the wall and lid caused by the sound pressure on the inside of the chamber. The power dissipated in this motion could be considered a loss to the system that would result in the lowered resonance amplitude of the chamber.

Figure 16 shows the effect of this attempt to stiffen the chamber walls on the measured acoustic response of the chamber. The addition of the steel rods produced no detectable change in the SPL measured inside the chamber (i.e., no improvement in absorption).

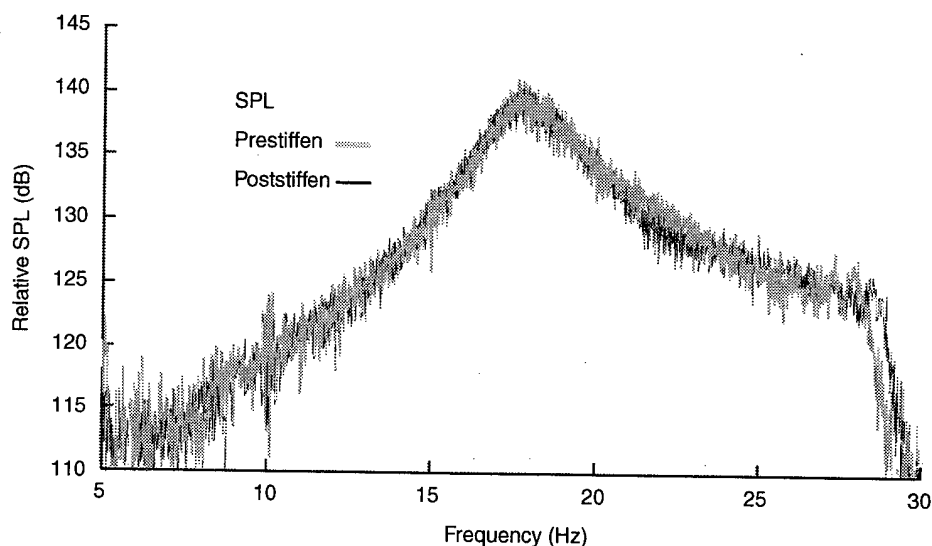
A general calculation to find the maximum bound on the power dissipation associated with a surface is to multiply the pressure P , the surface area of the surface in motion A_s , the deflection of the surface d_p , and the angular frequency of the deflection f :

$$P_{\text{surface}} = PA_s d_p (2\pi f) / \sqrt{2} . \quad (9)$$

We find the deflection of the surface by taking the double integral of the acceleration data with respect to time; this yields

$$d_p = a / (2\pi f)^2 , \quad (10)$$

Figure 16. Comparison of measured response of chamber with 23-in.-diam, 4-in.-long port attached before and after chamber was stiffened with steel rods.



where a is the measured peak acceleration at f . To calculate the total power dissipation associated with this deflection, we double P_{surface} to account for the opposite surface.

Table 3 lists the peak acceleration found from calculating the fast Fourier transform (FFT) of the data, the SPL in the chamber, and the resulting power dissipation.

We obtained the peak values in table 3 by performing FFTs on the measured data and recording the peak values of each FFT at the resonant frequency of 18 Hz. Representative FFTs of the SPL and wall and lid acceleration are shown in figure 17. The poor sensitivity of the accelerometers produced raw measured data that were very close to the noise floor of the recording equipment and may have produced some spurious results. Fortunately, the inherent narrow-band filtering of the FFT algorithm minimized the noise and produced reliable data. As expected, the data show a trend in the direction of increasing wall absorption and larger wall deflections at higher sound pressures. The calculated power loss by chamber wall flexure was not drastically changed by tightening of the braces. However, the calculated power losses under both conditions are very low. For instance, at 8 psig with the braces tightened, the calculated total power loss for the four largest surfaces in the chamber is just 3.6 W. This may be compared with a total acoustic power of about 3700 W impinging on those four surfaces. At a chamber Q of 3, this corresponds to a power dissipation of 1230 W. Evidently, the wall-deflection measurements cannot account for the acoustic chamber losses that we actually measured.

Our conclusion from this experiment is that the added steel rods caused only minor changes in the measured wall acceleration (displacement) and no detectable effect on the chamber's acoustic absorption. In hindsight this is not a surprising result. If a well-made (structurally rigid) chamber

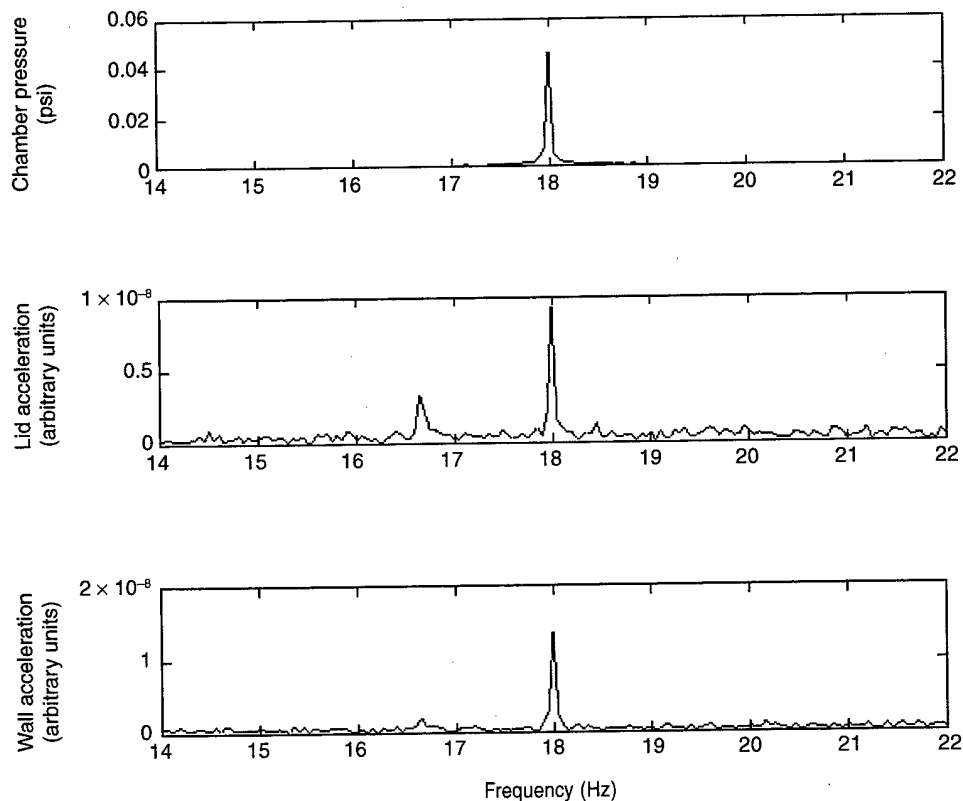
produces absorption coefficients on the order of 1 percent, and we are already seeing coefficients near 2 percent, then we would have had to have made substantial structural changes just to pick up an additional 1 percent absorption improvement.

Table 3. Peak measured wall acceleration at 18-Hz values and resulting calculated power loss in chamber walls.

| Brace status | Inlet pressure (psi) | Wall acceleration (m/s ²) | Lid acceleration (m/s ²) | Chamber pressure (Pa) | Power dissipation (4 surfaces) (W) |
|--------------|----------------------|---------------------------------------|--------------------------------------|-----------------------|------------------------------------|
| Loose | 6 | 0.0137 | 0.00932 | 319 | 0.28 |
| | 12 | 0.191 | 0.0519 ^a | 469 | 4.3 |
| Tightened | 2.7 | 0.0658 | 0.0664 | 223 | 1.1 |
| | 8 | 0.126 | 0.116 | 397 | 3.6 |
| | 12 | 0.137 | 0.127 | 480 | 4.9 |

^aThe low value may be erroneous; the FFT was unlike others measured at the same location.

Figure 17. A portion of FFTs of chamber wall accelerometer signals indicating magnitude of chamber sound pressure level at 18 Hz and responses of accelerometers to this force.



9. Loudspeaker Drive Experiment

As noted in section 7, we theorized that the excess acoustic losses in the chamber might result from the dc airflow through the chamber and port associated with the operation of the air compressor-modulator acoustic source. To explore this possibility and to verify the chamber response when it is driven by a *pure ac* sound source (no unidirectional airflow component), we performed a third experiment with the chamber driven by a loudspeaker rather than the MOAS source and modulator. We mounted a JBL 18-in.-diam low-frequency dynamic driver at one of the hatch openings in the chamber in place of the WAS 3000 modulator and drove this loudspeaker with audio-frequency sweep tones from 5 to 30 Hz to record the chamber response. Figure 18 shows the measured response (ragged solid curve) of the loudspeaker-chamber system with the tuning port closed (no chamber resonance).

Also shown in figure 18 is the predicted response (solid smooth curve) of the loudspeaker-driven chamber calculated with the chamber frequency-dependent wall-absorption value shown in figure 5. We calculated the predicted response from an electrical analog model similar to that discussed in section 3 for the modulator-driven system. A simplified schematic of this model is shown in figure 19. The loudspeaker equivalent loss, mass, and compliance were calculated from the published Thiele parameters for the JBL speaker used in the tests [5]. Above ~10 Hz the calculated response agrees reasonably well with the observed response, with the exception of an unexplained *kink* in the measured response at ~17 Hz. Figure 20 shows the measured and predicted (with frequency-dependent wall absorption) response of the loudspeaker-driven chamber to excitation of the 23-in.-diam port.

Even though no attempt was made in this test to maximize the SPL in the chamber (e.g., by applying the maximum allowable drive to the loudspeaker), we achieved a respectable continuous SPL in excess of 120 dB at 18 Hz using a simple audio power amplifier-loudspeaker combination as the audio signal source. *This simplified arrangement for the test chamber may be useful for effects testing at reduced sound intensities.* The measured response again shows a kink not predicted by the model. We also show a response curve calculated using a fixed value of 0.03 for the wall-absorption coefficient; if we ignore the kink, this curve is a reasonable match to the measured response and indicates an effective chamber Q of about 4.5. Therefore, the chamber Q and absorption measured with the loudspeaker drive is comparable to that measured with the modulator drive (table 2 and fig. 3), and we conclude that the dc airflow associated with the modulator did not cause substantial additional acoustic losses under our operating conditions. This experiment also indicates that the unexpectedly high acoustic losses we observed must be associated with the chamber rather than the acoustic driver.

Figure 18. Measured and modeled response of chamber with closed port excited by JBL 18-in. loudspeaker. Jagged solid curve is measured response; smooth curves are model responses calculated with initial (upper curve) and modified (lower curve) chamber absorption.

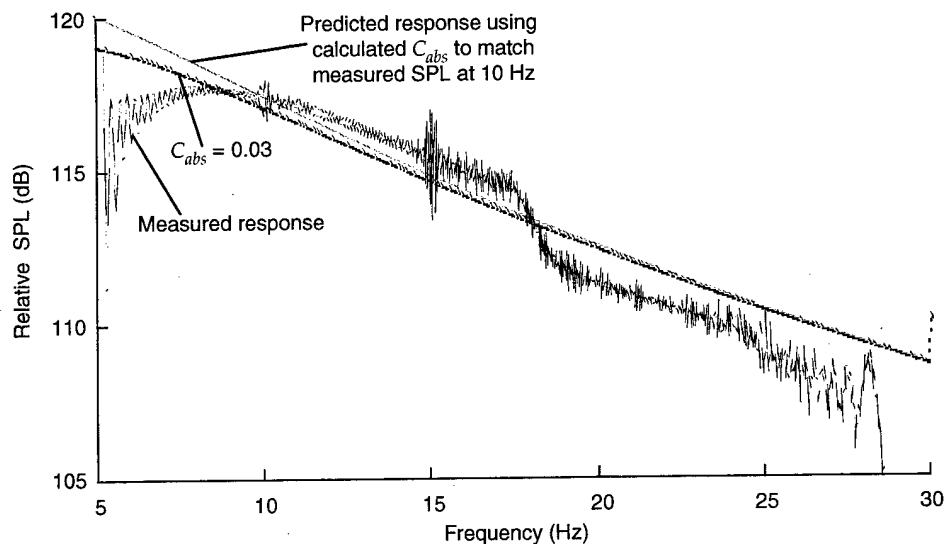


Figure 19. Electrical circuit analog of chamber driven by loudspeaker used for model calculations.

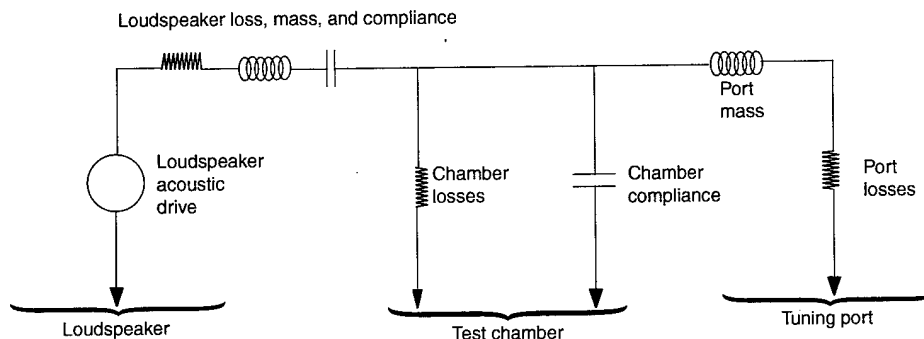
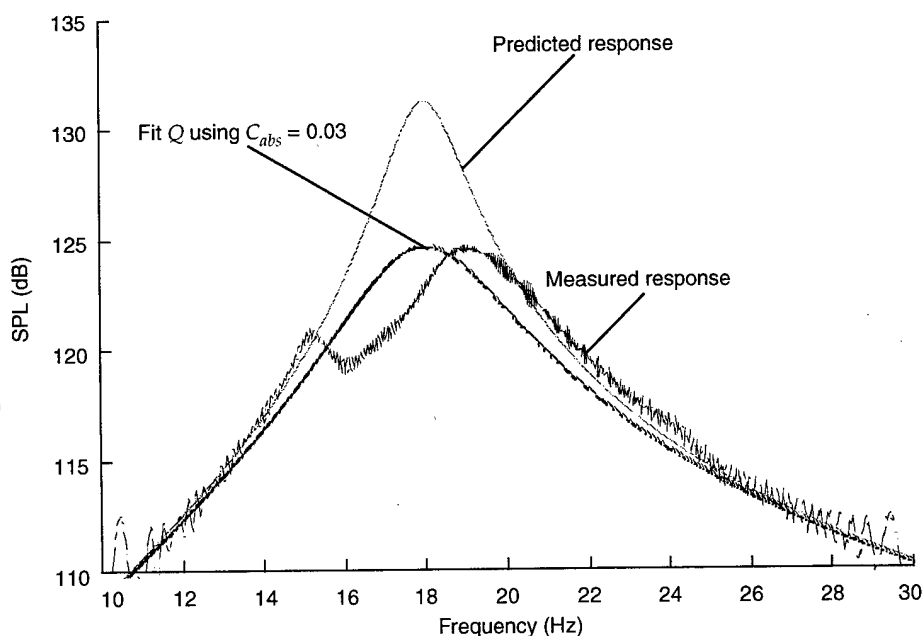


Figure 20. Measured and modeled response of chamber with 23-in.-diam, 4-in.-long port excited by JBL 18-in. loudspeaker. Jagged solid curve is measured response; smooth curves are model responses calculated with initial (upper curve) and modified (lower curve) chamber absorption.



10. Optimizing the Acoustic Intensity Within the Chamber

Current experiments have shown that we can develop SPLs of approximately 143 dB inside our experimental concrete test chamber driven by the MOAS source operating at its nominal conditions of 6 psig and 1200 cfm. The MOAS source is limited to a maximum pressure of 15 psig at 1890 cfm. At this level, we would induce a maximum SPL of approximately 148 dB: far less than our target SPL of >160 dB. The reason for the poor energy transfer is the substantial mismatch between the modulator impedance and the chamber impedance. Figure 21 shows that the acoustic impedance of the chamber when tuned to 18 Hz is approximately 2 k Ω . The WAS 3000 modulator on the other hand presents a very high impedance, over 67 k Ω , at its nominal operating parameters of 6 psig and 1200 cfm (fig. 22). The modulator is a high impedance device; it is designed to optimally couple to horns, which employ high throat impedance. (The horn that the WAS 3000 modulator normally drives employs a throat diameter of 4 in., which translates to an impedance of nearly 50 k Ω —not a bad match for the 67-k Ω modulator.) Figure 22 shows that the large impedance mismatch between the modulator (R_s) and the chamber is in effect a substantial voltage divider between the source and the chamber. To minimize this mismatch, the effective modulator impedance must be lowered to match the chamber impedance at resonance. *Therefore, the only way to extend the SPL above our 148-dB limit is to replace the WAS 3000 modulator with a modulator with a larger port area (lower acoustic impedance).*

A realistic minimum-impedance modulator (largest port area) that can operate within our frequency range would present an impedance in the low kilohm range. Using a modulator with a larger port area also gives us the opportunity to increase the capacity of our air supply. ARDEC has purchased a centrifugal blower air source that theoretically has the capacity to provide 3400 cfm at 28 psig. By using the centrifugal blower as the air source and a new modulator with a larger port area, we expect to generate SPLs inside the chamber in excess of 155 dB. One drawback to a new modulator, though, is that it would produce only pure continuous tones, whereas the WAS 3000 modulator is capable of producing complex modulated waveforms. To use the centrifugal blower air source with the WAS 3000 modulator does not appear feasible since the air temperature produced by the centrifugal blower would damage this modulator.

Figure 21. Acoustic impedance of chamber when tuned to 18 Hz.

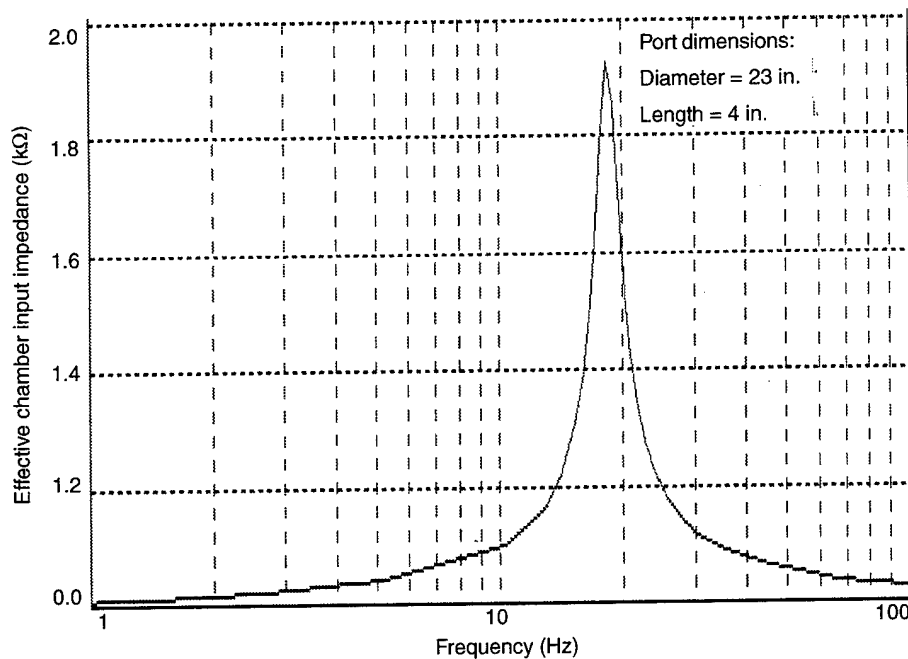
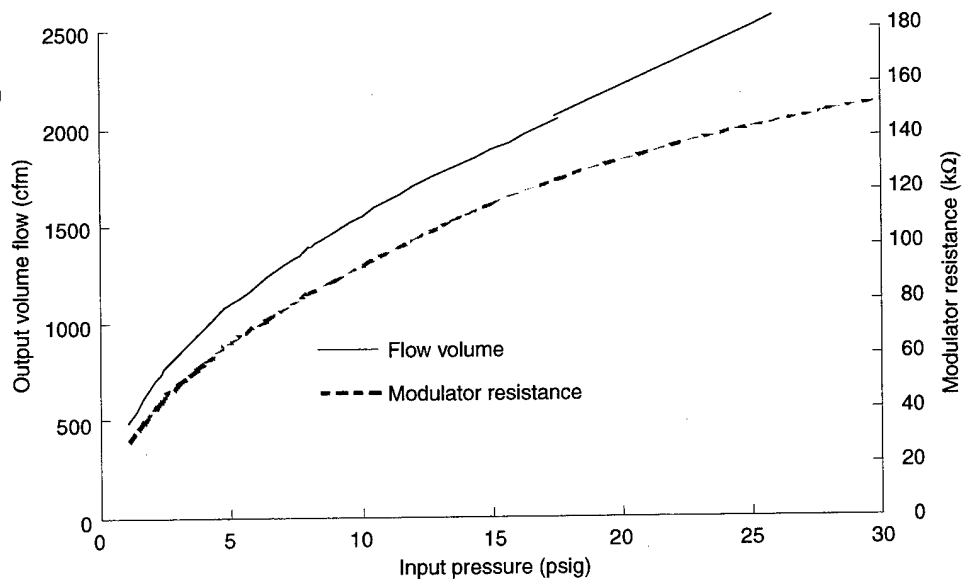


Figure 22. Volume flow and equivalent resistance of WAS 3000 air flow modulator as function of input pressure.



11. Conclusions

We have designed, modeled, constructed, and performed response measurements and analysis on a prototype acoustic test chamber intended to support high-intensity acoustic target-effects experiments at infrasonic frequencies. The experiments and analysis presented here have successfully demonstrated our design concept and show that we can generate high-intensity infrasonic sound pressure levels over a test volume large enough to accommodate complex experiments on large test items. Initial tests showed that SPLs of at least 143 dB could be generated over a frequency range of 5 to 20 Hz within a test volume of 5 m³. Modeling results indicate that further upgrades to the system (use of a high-capacity centrifugal blower air source, a specially designed low-impedance modulator, and an optimized chamber design) should allow us to extend the SPL to at least 155 dB. Finally, we note that continuous sound intensities near 120 dB were easily achieved in the prototype chamber when a simple power amplifier-loudspeaker combination was used as the audio signal source. This simplified arrangement for the test chamber may be useful for effects testing at reduced sound intensities. Table 4 summarizes our findings.

Table 4. Summary of measured and projected test chamber results.

| Source | Demonstrated SPL (dB) | Theoretical maximum (dB) | Complex modulation |
|--------------------------------------|-----------------------------|--------------------------------|-----------------------|
| Loudspeaker | 120 | 123 | Yes |
| MOAS | 143 | 148 | Yes |
| Centrifugal blower/ new modulator | — | 155 | No |

Acknowledgments

The authors wish to thank Bill Davis and Jack Kaiser of the Blossom Point Research Facility for their support for the field experiments, and John Noble and Mark Coleman of ARL for their interest and participation in the experiments with the ARL Mobile Acoustic Source. We also thank Harry Moore of TACOM/ARDEC for his continuing interest in this work.

References

1. L. L. Beranek, *Acoustics*, McGraw-Hill, New York (1954).
2. W. Seto, *Theory and Problems of Acoustics* (1971).
3. John Domen, TACOM/ARDEC, private communications (July-October 1998).
4. H. F. Olson, *Acoustical Engineering*, Van Nostrand, Princeton, NJ (1957), p 502.
5. D. B. Weems, *Designing, Building and Testing Your Own Speaker System*, McGraw-Hill, New York (1990).

Distribution

Admnstr
Defns Techl Info Ctr
Attn DTIC-OCF
8725 John J Kingman Rd Ste 0944
FT Belvoir VA 22060-6218

Ofc of the Secy of Defns
Attn ODDRE (R&AT)
The Pentagon
Washington DC 20301-3080

Ofc of the Secy of Defns
Attn OUSD(A&T)/ODDR&E(R) R J Trew
3080 Defense Pentagon
Washington DC 20301-7100

AMCOM MRDEC
Attn AMSMI-RD W C McCorkle
Redstone Arsenal AL 35898-5240

CECOM
Attn PM GPS COL S Young
FT Monmouth NJ 07703

Dir for MANPRINT
Ofc of the Deputy Chief of Staff for Prsnl
Attn J Hiller
The Pentagon Rm 2C733
Washington DC 20301-0300

TACOM/ARDEC
Attn AMSTA-AR-CCL-E C Freund
Attn AMSTA-AR-CCL-E L Sadowski
Attn AMSTA-AR-QAC K Yagrich
Attn AMSTA-AR-QAC T Hartmann
Attn AMSTA-AR-CCL-D H Moore (5 copies)
Picatinny Arsenal NJ 07806

US Army ARDEC
Attn AMSTA-AR-TD M Fisette
Bldg 1
Picatinny Arsenal NJ 07806

US Army Info Sys Engrg Cmnd
Attn ASQB-OTD F Jenia
FT Huachuca AZ 85613-5300

US Army Natick RDEC
Acting Techl Dir
Attn SSCNC-T P Brandler
Natick MA 01760-5002

US Army Simulation, Train, & Instrmntn
Cmnd
Attn J Stahl
12350 Research Parkway
Orlando FL 32826-3726

US Army Soldier & Biol Chem Cmnd Dir of
Rsrch & Techlgy Dirctr
Attn SMCCR-RS I G Resnick
Aberdeen Proving Ground MD 21010-5423

Engrg Ctr
Attn AMSTA-TR J Chapin
Warren MI 48397-5000

US Army Train & Doctrine Cmnd Battle Lab
Integration & Techl Dirctr
Attn ATCD-B J A Klevecz
FT Monroe VA 23651-5850

US Military Academy
Mathematical Sci Ctr of Excellence
Attn MDN-A LTC M D Phillips
Dept of Mathematical Sci Thayer Hall
West Point NY 10996-1786

Nav Surface Warfare Ctr A
Attn Code B07 J Pennella
17320 Dahlgren Rd Bldg 1470 Rm 1101
Dahlgren VA 22448-5100

DARPA
Attn S Welby
3701 N Fairfax Dr
Arlington VA 22203-1714

Hicks & Associates Inc
Attn G Singley III
1710 Goodrich Dr Ste 1300
McLean VA 22102

Distribution

Palisades Inst for Rsrch Svc Inc
Attn E Carr
1745 Jefferson Davis Hwy Ste 500
Arlington VA 22202-3402

Director
US Army Rsrch Ofc
Attn AMSRL-RO-D C Chang
PO Box 12211
Research Triangle Park NC 27709

US Army Rsrch Lab
Attn AMSRL-CI-AI-A Mail & Records Mgmt
Attn AMSRL-DD J Miller
Attn AMSRL-CI-AP Techl Pub (3 copies)
Attn AMSRL-CI-LL Techl Lib (3 copies)
Attn AMSRL-SE-D E Scannell
Attn AMSRL-SE-DE C Reiff
Attn AMSRL-SE-DS E Boesch Jr (20 copies)
Attn AMSRL-SE-DS H Brisker
Attn AMSRL-SE-DS J Tatum
Attn AMSRL-SE-DS L Jasper

| REPORT DOCUMENTATION PAGE | | | Form Approved OMB No. 0704-0188 | |
|--|---|--|--|---|
| Public reporting burden for this collection of information is estimated to average 1 hour per response, including the time for reviewing instructions, searching existing data sources, gathering and maintaining the data needed, and completing and reviewing the collection of information. Send comments regarding this burden estimate or any other aspect of this collection of information, including suggestions for reducing this burden, to Washington Headquarters Services, Directorate for Information Operations and Reports, 1215 Jefferson Davis Highway, Suite 1204, Arlington, VA 22202-4302, and to the Office of Management and Budget, Paperwork Reduction Project (0704-0188), Washington, DC 20503. | | | | |
| 1. AGENCY USE ONLY (Leave blank) | | 2. REPORT DATE April 2000 | | 3. REPORT TYPE AND DATES COVERED 6/98-3/99 |
| 4. TITLE AND SUBTITLE Design and Test of a Prototype Acoustic High-Intensity Infrasonic Test Chamber | | | 5. FUNDING NUMBERS DA PR: A140 PE: 62120A | |
| 6. AUTHOR(S) H. Edwin Boesch, Jr., Bruce T. Benwell, and Christian G. Reiff | | | | |
| 7. PERFORMING ORGANIZATION NAME(S) AND ADDRESS(ES) U.S. Army Research Laboratory Attn: AMSRL-SE-DS email: eboesch@arl.mil 2800 Powder Mill Road Adelphi, MD 20783-1197 | | | 8. PERFORMING ORGANIZATION REPORT NUMBER ARL-TR-2137 | |
| 9. SPONSORING/MONITORING AGENCY NAME(S) AND ADDRESS(ES) TACOM/ARDEC Picatinny Arsenal Dover, NJ 07806-3000 | | | 10. SPONSORING/MONITORING AGENCY REPORT NUMBER | |
| 11. SUPPLEMENTARY NOTES ARL PR: 0NEYYY AMS code: 622120.140 | | | | |
| 12a. DISTRIBUTION/AVAILABILITY STATEMENT Approved for public release; distribution unlimited. | | | 12b. DISTRIBUTION CODE | |
| 13. ABSTRACT (Maximum 200 words) We describe the conception, design, mathematical modeling, construction, and test of a prototype acoustic test chamber intended to support the performance of high-intensity acoustic target-effects experiments on large targets at infrasonic frequencies. In initial experiments, the test chamber produced continuous sinusoidal sound pressure levels in excess of 140 dB over a frequency range of 5 to 20 Hz within a test volume of 5 m ³ . | | | | |
| 14. SUBJECT TERMS Infrasound, Helmholtz, resonator, high-intensity sound | | | 15. NUMBER OF PAGES 39 | |
| | | | 16. PRICE CODE | |
| 17. SECURITY CLASSIFICATION OF REPORT Unclassified | 18. SECURITY CLASSIFICATION OF THIS PAGE Unclassified | 19. SECURITY CLASSIFICATION OF ABSTRACT Unclassified | 20. LIMITATION OF ABSTRACT SAR | |